Journal of Alloys and Compounds 501 (2010) 6–13

Contents lists available at ScienceDirect

Journal of Alloys and Compounds

journal homepage: www.elsevier.com/locate/jallcom

Polycrystalline PbSe on a polyimide substrate

G. Radovsky[a], Z. Dashevsky[a,*], V. Kasiyan[a], M. Auslender[b,**], S. Hava[b]

[a] Department of Materials Engineering, Ben Gurion University of the Negev, POB 653, Beer Sheba 84105, Israel
[b] Department of Electrical and Computer Engineering, Ben Gurion University of the Negev, POB 653, Beer Sheba 84105, Israel

ARTICLE INFO

Article history:
Received 7 February 2010
Accepted 4 April 2010
Available online 18 April 2010

Keywords:
Semiconductors (IV-VI)
Thin films
Optical materials
Vapor deposition
Electrical transport
Grain boundaries
Optical properties
X-ray diffraction
SEM
AFM
Optical spectroscopy
Light absorption and reflection
Computer simulations

ABSTRACT

In addition to the films of lead salts used in the photoconductive IR detectors, we quest for the polycrystalline films appropriate to the photovoltaic detectors. This work focues on PbSe, for it exhibits Auger coefficient much lower than HgCdTe and still lower compared to PbTe. To provide thermal and mechanical stability, we chose a pseudo-crystalline polyimide for being the films deposition substrate. Various regimes regarding the substrate temperature at the deposition process, and its duration managing the film thickness, were probed. The films were characterized structurally and morphologically. To determine the type of carriers, their concentration and mobility, effect of Hall and electrical conductivity were measured in the range 77–300 K. To infer on the optical quality of the films, the IR reflectance and transmittance spectra at 300 K were measured in the range 1–5.3 μm. These diverse characterizations allowed us to find a regime optimal for growing the films with good grain crystallinity and relatively small surface roughness. Using optical bi-layer model, we showed that the measured IR spectra of these films are compatible with some effective-medium complex refractive index, the extracted effective band gap energy being about the same as that for bulk PbSe.

1. Introduction

Lead salts PbX (X = S, Te, Se) have narrow band gaps corresponding to the wavelengths $\lambda \sim 3.0\,\mu m$ (PbS), 3.9 μm (PbTe), 4.3 μm (PbSe) at 300 K, see e.g. [1,2]. Therefore, for over a century they remain materials of high interest for detection, including molecular and gas spectroscopy [3], and the emission – lasing and photoluminescence (PL) in the mid infrared (IR) [4]. Polycrystalline PbX photoconductive detectors (PCD) show nearly constant peak detectivity over the range 77–193 K, comparable to that at 77K of similar PCD based on HgCdTe in the respective spectral ranges [3]. At 295 K their detectivity gets notably smaller, but remains high enough to make the PbX based PCD preferable to detectors requiring a cooling system. By other scores, photovoltaic (PV) devices, e.g. p–n and Schottky junction photodiodes seem mostly advantageous for the IR detection [3]. Their fabrication is possible with: (i) high quality single crystalline film or bulk samples; (ii) polycrystalline films with the grains micron-scale size and a good crystallinity.

The singe crystalline PbX films became available with the advent of modern epitaxial growth techniques, such as LPE, HWE and MBE ones [2]. Efficient operation of the polycrystalline PbX based PCD at high temperature was hoped to remain to their single crystalline PV counterparts and quantum effect devices as well, and this expectation came true [3–5]. The noted superiority of PbX based PCD is in part due to their Auger coefficient, smaller than that of II–VI (e.g. HgCdTe) and some III-V semiconductors. It is known both theoretically [6] and experimentally [7] to vary weakly with the temperature in the 77–295 K range. However, the key issues with those PCD are the preparation and post-growth sensitization (since as grown PbX films are not photosensitive), which were not well understood and could only be reproduced with well-tried recipes. Still, not all types of the films are sensitized by the post-growth treatments. The sensitivity, structure, electrical transport and carrier recombination mechanisms issues for the sensitized films are not completely resolved that stimulates continuing the research [8]. On the contrary, fabricating the single crystalline IV–VI films was elaborated to such state of art [4,5] that they were in serious competition with HgCdTe for developing the detectors. However, transferring the knowledge to commercial foundries was stopped to the end of 1980s because PbX suffer from two drawbacks seemed significant. One is very high thermal expansion coefficient precluding direct epitaxial growth, except that on crystalline BaF_2. In the

* Corresponding author. Tel.: +972 86472573; fax: +972 86472946.
** Corresponding author. Tel.: +972 86461583; fax: +972 86472949.
E-mail addresses: zdashev@bgu.ac.il (Z. Dashevsky), marka@ee.bgu.ac.il (M. Auslender).

0925-8388/$ – see front matter © 2010 Elsevier B.V. All rights reserved.
doi:10.1016/j.jallcom.2010.04.064

end of 1980s, Zogg et al. [4] started to grow the epitaxial PbTe on silicon, using a CaF_2/BaF_2 buffer layer, to overcome the mismatch problems. They continued to pursue this technology and made such significant progress [5] that nowadays the thermal and lattice mismatches would not be fundamental limitations either. The PbTe PV arrays by Zogg et al. [4,5] offered considerable advantages compared to HgCdTe ones as regards the manufacture ease, homogeneity and costs [3].

For fabricating the photosensitive films, the above noted mismatches are just useful, as they favorite growing the polycrystalline films with very small grains, which are well photosensitized by an oxygen annealing [8]. For example, upon an initial evaporation of PbSe on a SiO_2/Si substrate the grains are of few tens nanometer mean size; extra iodine annealing re-crystallizes the film while the grain grow up, but their mean size does not finally exceeds 300 nm [9]. Substrates with lattice mismatch, smaller than for SiO_2, were tried to grow large-grain polycrystalline films, e.g. PbTe on mica, and BaF_2 with smallest known mismatch, were reported [10]. For the PV applications, however, these substrates are impractical due to poor metallization, solubility in water (BaF_2) and the film cracking (except BaF_2) at mild cooling still needed in the PV devices.

At present, PbSe is attracting renewed growing interest because it exhibits still lower Auger coefficient compared to PbTe, which should lead to better performance of PV, and lower threshold power of the PL and lasing devices. Room-temperature PL reported long ago [11] for polycrystalline PbSe films, has been revisited recently [12]. Strikingly, PL from bulk like MBE PbSe films was shown [13] to persist up to 190 °C, which was not met so far in any quantum effect emitter. Very recently, a PbSe/PbEuTe resonance-cavity enhanced laser operating above room temperature has been reported [14]. At the same time, there has not been any niche for the large-grain PbX based PV detectors, so it is timely to explore this alternative to the existing single crystalline based ones. It worth emphasizing that in this case a key problem is the choice of practical substrate as no one has been known yet, whereas technologies of fabricating the vertical p–n and Shottky junctions in polycrystalline films are well known since early 1980s [15], see also another option for PbTe [10]. Hence, we first looked for a substrate which would provide mechanical and thermal stability as well as backside metallization, and found Kapton® polyimide [16] to be most appropriate for this purpose.

The present paper reports on the growth and characterization of the PbSe films on the polyimide substrate. We describe an optimal deposition regime under which a series of high quality films was obtained. In addition to structural characterization revealing good crystallinity of the grains and relatively small surface roughness, these films adopt an advanced electrical and optical characterization from which basic material parameters can be extracted.

2. Experimental details

Polycrystalline PbSe films were grown by an electron beam assisted Edwards E306A (10^{-5} mbar vacuum) Physical Vapor Deposition (PVD) system. The film thickness was managed by the deposition time, the deposition rate being about 0.1–0.2 nm/s. The film morphology, i.e. the mean grain size and surface roughness, depend on the substrate temperature T_s kept to within ±3 °C, as a result of the deposition conditions. To determine a PVD regime yielding the best structural, transport and optical properties, several few T_s in the range −50 to 350 °C were probed. For $T_s \geq 100$ °C, an attached heater was used. T_s below 100 °C were achieved by cooling with liquid nitrogen. Yet, the heating well above 250 °C was ruled out at an early stage, because the properties of the polyimide required for PVD do not withstand such conditions.

For the phase and texture characterization, we employed a X-ray Rigaku Model-2000 diffractometer operating with Cu Kα radiation (λ = 1.5405 Å) at 40 kV and 30 mA. The X-ray diffraction (XRD) spectra are shown in Fig. 1. The films morphology was assessed using a JEOL JSM-5600 SEM with an accelerating voltage 15 kV. Because of a specific conductivity mechanism, a metallic coating is needed for obtaining good-contrast SEM images. To this end, we used a few tens nanometer thick Au layer. The surface structure was analyzed by AFM at ambient conditions using a Thermo-microscopes CP Research instrument in an intermittent contact mode with a scan rate of 0.25–1 Hz. The SEM and AFM images of several samples are shown in Figs. 2 and 3, respectively.

For transport measurements, electrical contacts were prepared from nickel by thermal evaporation. For all samples, the contacts proved Ohmic, which is confirmed by the linear current–voltage relation over the examined temperature range 80–300 K. The electrical conductivity at zero magnetic induction, and the effect of Hall at 2 Tesla, were measured. IR optical properties were probed in the spectral range from 1 to 5.3 μm using a setup on the base of a Horiba FHR640 monochromator with the resolution of 0.016 nm. Tungsten halogen lamp, sparked at 250 W was a light source and the radiation was mechanically chopped at 140 Hz using TTT C995 chopper controller. To detect the transmitted and reflected radiation, an InSb photodiode cooled down to 77 K was used. After a SR 7265 DSP amplifier, the recorded signals were collected using Lab-View program. For the normal-incidence transmittance measurements, samples were put into a standard holder. Angular reflection was obtained using high-precision Bruker grazing angle unit supplied with golden-mirror reference (about 100% reflectivity in the whole measurement range), which allows varying the incidence and scattering angles from 10° to 80°.

3. Theory

For the consideration of electric transport in the fabricated films, we use well known formulas for the conductivity σ and Hall coefficient R_H of an unipolar semiconductor, which include the carrier concentration (n or p), conductivity effective mass (m_c) and the relaxation time (τ). For the anisotropic parabolic band structure of PbX [2]

$$m_c = 3\left(\frac{2}{m_t} + \frac{1}{m_l}\right)^{-1}, \tag{1}$$

where m_t is the transverse and m_l the longitudinal effective mass; in n- and p-type PbSe, m_c equals $0.0466m_0$ and $0.0408m_0$, respectively [2]. According to the Drude formula [17], the carriers contribution to the dielectric susceptibility of the semiconductor is given by

$$\delta\varepsilon_r(\omega) = -\frac{\omega_p^2}{\omega(\omega + (i/\tau))}, \tag{2a}$$

where

$$\omega_p = \sqrt{\frac{Nq^2}{\varepsilon_0 m_c}} \quad (N = n, p) \tag{2b}$$

is the plasma frequency, q being the electron charge and ε_0 is the free space permittivity.

Optically, polycrystalline samples with the mean crystallite size smaller than light wavelength are well described by an effective homogeneous dielectric susceptibility [18]. Within this effective-medium approach our samples are optical bi-layers in which a thin film, described by an effective complex refractive index $n_1 + ik_1$, covers a partially transparent thick substrate, described by a true complex refractive index $n_2 + ik_2$ where $k_2 \ll n_2$. For this structure, analytical calculation of the reflectance $\mathcal{R}$ and transmittance $\mathcal{J}$ using well-known method is possible [19], which gives

$$\mathcal{R} = \left| \frac{\rho_{01} + \rho_{12}e^{2i\phi_1} + (\rho_{01}\rho_{12} + e^{2i\phi_1})\rho_{20}e^{2i\phi_2}}{1 + \rho_{01}\rho_{12}e^{2i\phi_1} + (\rho_{12} + \rho_{01}e^{2i\phi_1})\rho_{20}e^{2i\phi_2}} \right|^2 \tag{3}$$

and

$$\mathcal{J} = \left| \frac{(1 + \rho_{20})(1 + \rho_{12})(1 + \rho_{01})e^{i(\phi_1 + \phi_2)}}{1 + \rho_{01}\rho_{12}e^{2i\phi_1} + (\rho_{12} + \rho_{01}e^{2i\phi_1})\rho_{20}e^{2i\phi_2}} \right|^2. \tag{4}$$

In Eqs. (3) and (4) ρ_{jl} is the complex Fresnel reflection amplitude at interface between the media j and l (0 denotes the air), and ϕ_j is the complex optical phase acquired by the light wave traversing the layer j having a thickness d_j, given by

$$\rho_{jl} = \frac{n_j + ik_j - n_l - ik_l}{n_j + ik_j + n_l + ik_l}, \quad \phi_j = \frac{2\pi(n_j + ik_j)d_j}{\lambda}. \tag{5}$$

When the optical thickness of the substrate satisfies the inequality $d_2/n_2 \gg \lambda$ the spectra calculated using Eqs. (4) and (5) show the interference fringes with the wave-number period $1/(2n_2d_2)$,

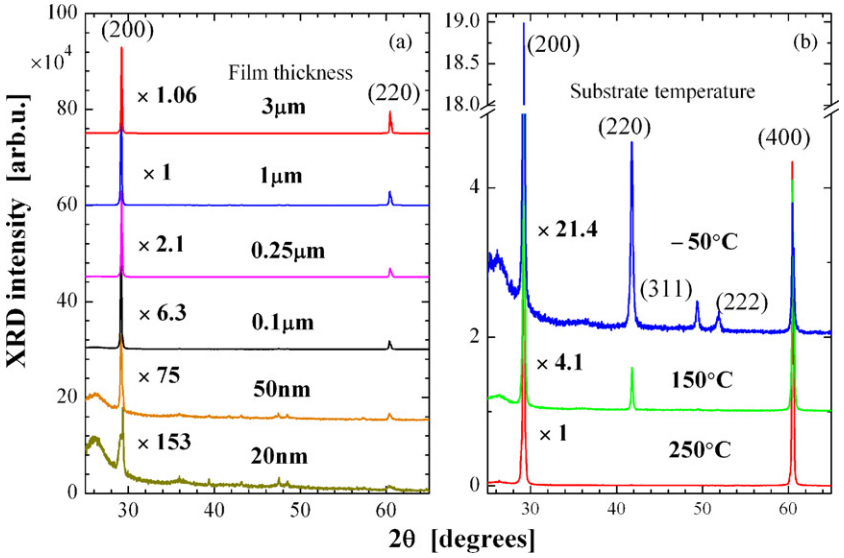

Fig. 1. XRD spectra of the polycrystalline PbSe films. The strongest (2 0 0) peak intensity is taken for normalization the same for all samples. (a) The substrate temperature is T_s = 250° C and thickness d_f varies as shown in the figure. (b) The films thickness is d_f = 3 μm and the substrate temperature T_s varies as shown in the figure.

which should be resolved with our monochromator, and be intense since $k_2/n_2 \approx 7 \times 10^{-3}$ at most for the polyimide. Actually, in the measured spectra the fringes are small compared to the theoretical ones as seen from inset in Fig. 6(b). The reason for that is the scattering by imperfections in the bulk, which breaks down the coherence of the light waves reflected from the interfaces back into the substrate. If one describes this scattering by random fluctuations of n_2, the statistical average of $\mathcal{R}$ and $\mathcal{J}$ is equivalent to their average over the optical-path phase $\Phi = \mathrm{Re}(\phi_2)$, which is mathematical idea behind the multiple-reflection approximation [20]. For one thick slab in the air, the well known apparent transmittance formula obtained [17] by an incoherent summation of the multiply reflected rays, indeed follows from such an averaging. While for our structure the ray picture is too much complex, the analytical averaging over Φ still remains possible. The results for the apparent reflectance and transmittance are given by

$$\mathcal{R}_a = \langle \mathcal{R} \rangle_\Phi = \left| \frac{\rho_{01} + \rho_{12} e^{2i\phi_1}}{1 + \rho_{01}\rho_{12} e^{2i\phi_1}} \right|^2 + \left| \frac{(\rho_{12}^2 - 1)(\rho_{01}^2 - 1)\rho_{20} e^{2i(\phi_1+\phi_2)}}{(1 + \rho_{01}\rho_{12} e^{2i\phi_1})^2} \right|^2 \times \frac{1}{1 - |((\rho_{12} + \rho_{01} e^{2i\phi_1})/(1 + \rho_{01}\rho_{12} e^{2i\phi_1}))\rho_{20} e^{2i\phi_2}|^2}, \quad (6)$$

$$\mathcal{J}_a = \langle \mathcal{J} \rangle_\Phi = \frac{|((1+\rho_{01})(1+\rho_{12})(1+\rho_{20}) e^{i(\phi_1+\phi_2)})/(1 + \rho_{01}\rho_{12} e^{2i\phi_1})|^2}{1 - |((\rho_{12} + \rho_{01} e^{2i\phi_1})/(1 + \rho_{01}\rho_{12} e^{2i\phi_1}))\rho_{20} e^{2i\phi_2}|^2}. \quad (7)$$

Eqs. (4)–(7) are valid if non-specular scattering due to the surface roughness does not dominate the transmission and reflection.

4. Results and discussion

4.1. Structural properties

We grew the PbSe films with thicknesses d_f in the range 0.02–3 μm upon the 100 μm polyimide substrate. Table 1 presents the films along with their structural parameters; for $d_f \leq 3$ μm, a unique T_s = 250 °C was applied. For d_f = 3 μm, there are four samples corresponding to T_s = −50, 100, 150 and 250 °C. Fig. 1(a) displays the XRD spectra of samples with T_s = 250° C for the selected d_f values, as shown on the figure. The (2 0 0) and (4 0 0) Bragg peaks typical for rock-salt structure of PbSe are clearly seen on the spectra even for smallest d_f = 20 nm. The high intensity of the (2 0 0) peak and higher order (4 0 0) one, in conjunction with the suppression of other peaks from the XRD standard of PbSe, indicates that the growth occurs in the preferred orientation even at an early nucleation stage. Impurity phases such as Pb, Se, SeO_2, PbO, $PbSeO_3$ and $PbSeO_4$ are not observed in the XRD patterns, which confirms one-phase nature of these films. We estimated the penetration depth of the used X-rays to be ∼6 μm, and therefore we attributed few small, independent of T_s peaks to an XRD pattern from incompletely amorphous polyimide (not shown).[1] Fig. 1(b) shows the variation of the XRD spectra of the 3 μm films with the variation of T_s. It appears that the (2 0 0) XRD peak intensity dominant at T_s = 250 °C, see Fig. 1(a), decreases with decreasing T_s both absolutely, and relatively to the intensity of other peaks from the PbSe XRD standard. In particular, the (2 2 0), (3 1 1) and (3 2 2) peaks become substantial at T_s < 100 °C. This trend is explained [21] by decreasing the ad-atoms mobility with the decrease of T_s that manifests itself in the gradual loss of the preferred orientation. For the films presented in Fig. 1(a), except one with d_f = 0.02 μm, the XRD spectra have ∼0.16° 2θ-FWHM compatible with ∼0.06° θ-FWHM of rocking curve for MBE PbSe [5], which proves a good crystallinity of the grains. This feature reflects the fact that at early grain nucleation stage, the crystal lattice may distort towards partial grain amorphization due to a mismatch between the substrate and growing film. As the film thickens beyond 20 nm, the strain relaxed grains grow on the existing strained ones, which

Table 1
The PbSe polycrystalline films, their fabrication conditions and structural parameters; T_s – deposition temperature, d_f – film thickness, RMS abbreviates rooted mean square, SEM/AFM means the methods by which the grain size was estimated.

Sample	T_s (°C)	d_f (μm)	Grain size (nm)	RMS roughness (nm)
1	250	0.02	60 AFM	2.86
2	250	0.05	95 AFM	2.4
3	250	0.1	135 AFM	2.35
4	250	0.25	115 SEM	–
5	250	1	300 AFM	32
6	250	1.5	360 SEM	–
7	250	2	430 SEM	–
8	250	3	590 AFM	45.4
9	150	3	590 AFM	108
10	100	3	590 AFM	165.3
11	−50	3	590 AFM	256.4

[1] The polyimide derived peaks are hardly seen in Fig. 1 (a) for $d_1 \geq 0.1$ μm because of drastic increase of the (200) peak intensity and the adopted normalization procedure, see caption to Fig. 1(a).

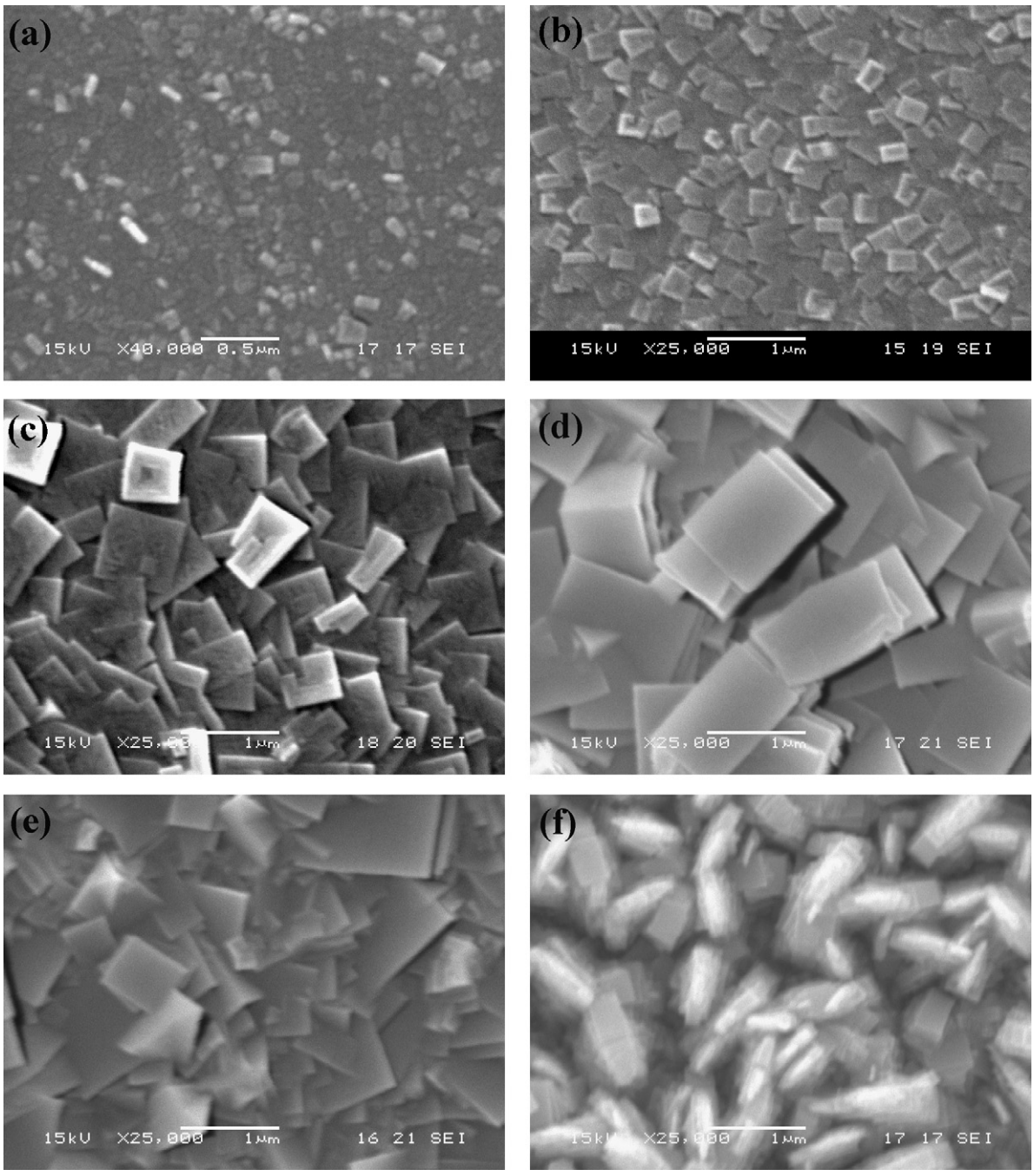

Fig. 2. SEM images of the polycrystalline PbSe films. The substrate temperature is $T_s = 250^\circ$ C and thicknesses d_f are: (a) 0.25 μm; (b) 1 μm; (c) 3 μm. The thickness is $d_f = 3$ μm and the substrate temperatures T_s are: (d) 150 °C, (e) 100 °C, (f) −50 °C.

results in drastic narrowing of the XRD spectra. For other T_S probed, the XRD spectra prove notably wider than those discussed above for $T_s = 250$ °C.

Fig. 2(a)–(c) show the microstructure of the films with three different thicknesses grown at $T_s = 250$ °C. These SEM images reveal three-dimensionally grown submicron sized PbSe crystallites and demonstrate clear correlation between the mean crystallite size and the film growth time, i.e. the thickness d_f. Fig. 2(c)–(f) present the changes in the microstructure with the change of T_s. It is seen that lowering T_s results in increasing the surface roughness and the number of voids because the self-diffusivity of ad-atoms decreases. Thus many grains coalesce during the film thickening and surface topography becomes more accentuated; for details see review [21]. Fig. 2 shows that the crystallites are either interlocked or aggregated with each other. Therefore, it is difficult to accurately measure their dimensions with SEM alone. By this reason, AFM was employed with the aid of Thermo-microscopes Pro Scan Image Processing software to estimate the mean grain size from large numbers of topography images. Fig. 3(a)–(c) show the evolution of the surface roughness with d_f for $T_s = 250$ °C. It appears that starting from $d_f = 0.1$ μm the roughness is proportional to d_f, but for $d_f \geq 1$ μm its increase slows down drastically, see Table 1, and compare Fig. 3(a) with Fig. 3(b) and the latter with Fig. 3(c) as well. Also, a strong roughness increase with decreasing T_s is evident from Fig. 3(c)–(f). The data of Table 1 predicts nearly linear dependence of the roughness on T_s.

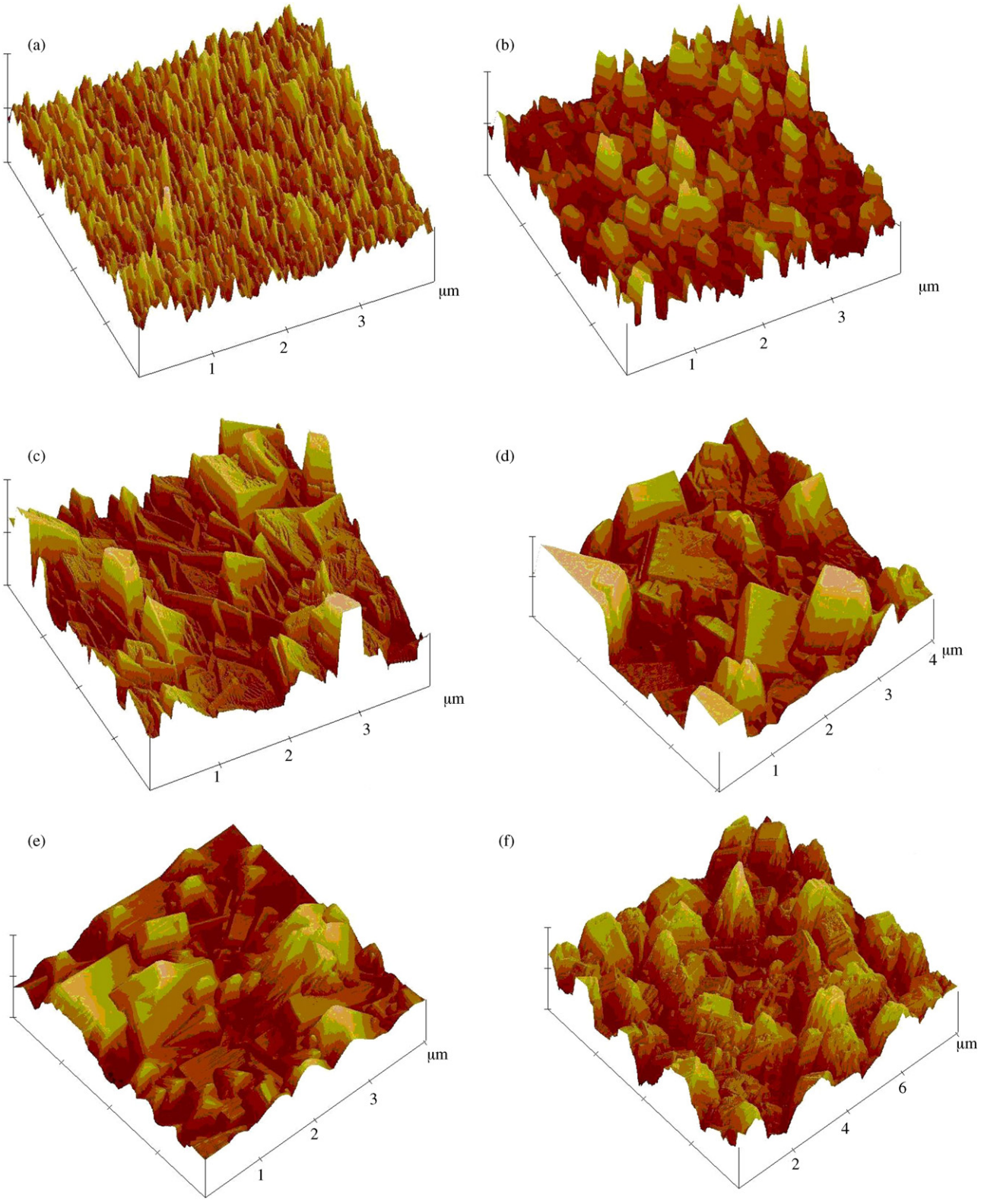

Fig. 3. AFM images of the polycrystalline PbSe films. The roughness is shown in Table 1. The substrate temperature is T_s = 250 °C and thicknesses d_f are: (a) 0.1 μm; (b) 1 μm; (c) 3 μm. The thickness is d_f = 3 μm and the substrate temperatures T_s are: (d) 150 °C, (e) 100 °C, (f) −50 °C.

4.2. Transport properties

From measured R_H we inferred that all our films are of p-type with the concentration of holes weakly dependent on temperature, varying from sample to sample in the range $p \sim 0.9–1.9 \times 10^{19}$ cm^{-3}. With measured σ the Hall mobility was determined, as usually, by $\mu = R_H\sigma$. Fig. 4 shows the temperature dependence of μ for all 3 μm thick films presented in Table 1. It is seen that μ is lower by three and two orders of magnitude at low and room temperature, respectively, than that for single crystals

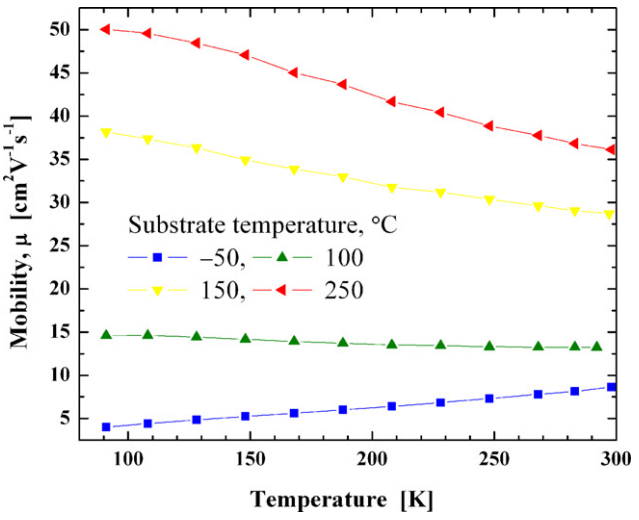

Fig. 4. The mobility in the 3 μm thick films, deposited at various T_s as shown in the figure, vs. the temperature, lines are guides for eye.

[2,22]. Also, given the sample temperature, the lower T_S the smaller μ. While in all samples, except one with $T_s = -50\,^{\circ}$C, μ decreases with increasing the temperature. For $T_s = -50\,^{\circ}$C, μ behaves different, namely increases with increasing the temperature. When the decrease of μ takes place, its rate strengthens with increasing T_s (see Fig. 4). The observed temperature dependence of μ can be explained by domination of the grain boundaries effects in the electric transport [8] in a marked contrast with bulk single crystals in which the high-mobility band transport is dominated by the lattice scattering [2,22]. Apart from the $T_s = -50\,^{\circ}$C case, it would be reasonable to assume the Mattissen rule

$$\frac{1}{\mu} = \frac{1}{\mu_{gb}} + \frac{1}{\mu_{ph}}, \tag{8}$$

where μ_{gb} and μ_{ph} is the mobility due to scattering by grain-boundaries and phonons, respectively; usually μ_{gb} is constant and $\mu_{ph} \propto T^{-a}$. With this prescription, Eq. (8) fits well the measured temperature dependence. The best fit (not shown) yields at $T_s = 250\,^{\circ}$C, $\mu_{gb} = 55 \pm 1$ cm^2/V-s, and $a = 1.6 \pm 0.2$ which is close to the exponent for PbSe single crystals [2]. Note that the above limiting mobility agrees well with $\mu = 53$ cm^2/V-s reported for 50–100 nm grain size p-type PbTe films with $p \sim 2 \times 10^{17}$ cm^{-3} [23]. For $-50\,^{\circ}\text{C} < T_s < 250\,^{\circ}$C, we obtained $a \approx 1$ with the worse fit quality. Similar exponent in single crystals is attributed to heavy doping [2,22], but in our case it may result also from interference of the above two mechanisms occuring if the grain-boundary scattering is strong enough. For the films with $T_s = -50\,^{\circ}$C, μ exhibits an activation character which may be explained by inter-grain hopping of the carriers. For $T_s = -50\,^{\circ}$C, our data fits well a model by Sheng et al. [24]

$$\mu = \mu_0 \ \exp\left(-\sqrt{\frac{E_0}{kT}}\right), \tag{9}$$

where E_0 is grain recharge energy in the hopping process and T is absolute temperature. The best fit (not shown) at a low temperature region results in the following parameters: $E_0 = 13 \pm 1$ meV, $\mu_0 = 14.2 \pm 0.4$ cm^2/V-s. The small value of E_0 agrees well with high static dielectric constant of PbSe [1,2].

4.3. Optical properties

The near-normal (10° incidence) reflectivity and normal transmittance spectra of the fabricated films are shown in Figs. 5 and 6,

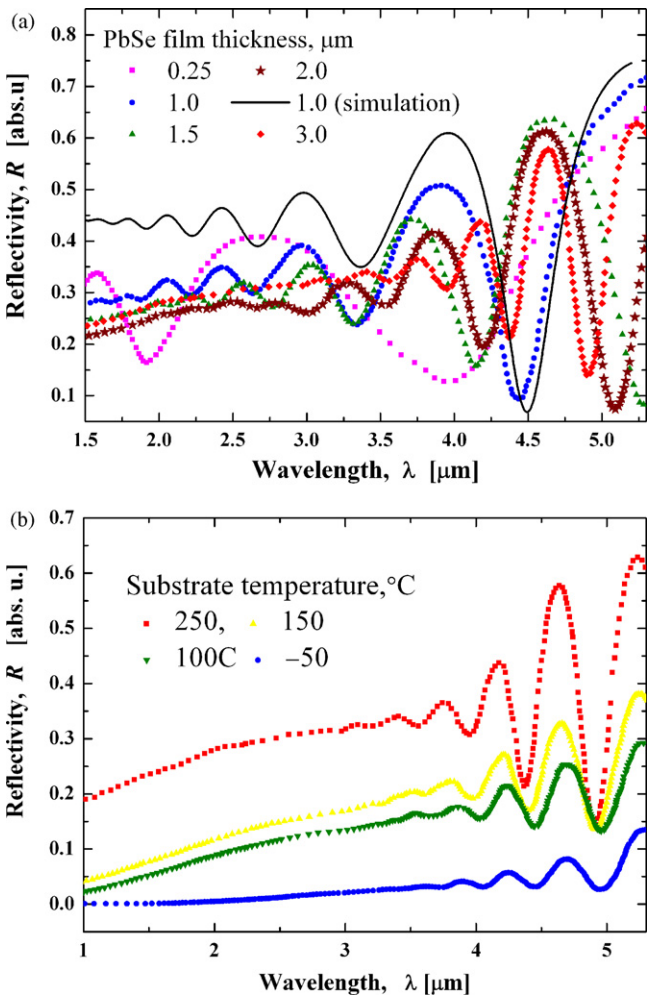

Fig. 5. The reflectivity spectra of the polycrystalline PbSe films. (a) $T_s = 250\,^{\circ}$C and d_f varies as shown in the figure; (b) $d_f = 3$ μm and T_s varies as shown in the figure.

respectively. High resolution measurements do reveal the substrate related interference fringes but, as seen from the inset in Fig. 6(b), with the amplitude much smaller than the theoretical prediction via Eqs. (3)–(5). As it is impossible to quantify the coherence suppression related to the substrate, we eliminated the fringes by reducing the λ resolution, and thus analyzed the experimental data using smoothed Eqs. (6) and (7). For the analysis, we first extracted the optical constants n_2, k_2 of the substrate, using the reflection and transmission spectra from bare polyimide obtained before the PbSe deposition, and the well-known analogs of Eqs. (6) and (7) for $\mathcal{R}_a$ and $\mathcal{J}_a$, respectively, of one slab in the air.

Figs. 5(a) and 6(a) shows the reflection and transmission spectra, respectively, of the films with various thicknesses deposited at $T_s = 250\,^{\circ}$C, see also Table 1. It appears that the data obey the regularities predicted by Eqs. (6) and (7). For example, the well known reflectance oscillations due to optical interference in the thin film, when increasing the film thickness increases the wavenumber period of the oscillations, is clearly seen in Fig. 5(a). It is seen also that lowering λ decreases the oscillations amplitude that originates from the increase of the IR absorption. The thinner the film the shorter λ of the suppression onset of the oscillations, as less beam intensity is absorbed in each single pass. In a marked contrast, the film related oscillations of the transmittance are much less pronounced and seen only at $\lambda > 3.5$ μm (not shown). Below this threshold the polyimide and PbSe film related IR absorption dominates the transmission. Though the fundamental IR absorp-

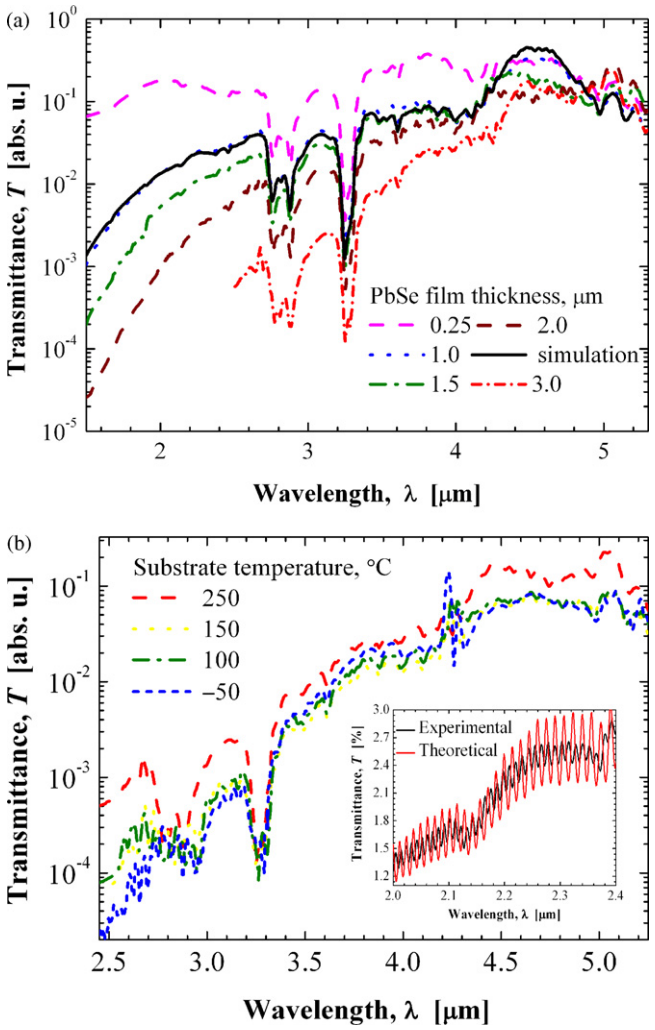

Fig. 6. The transmittance spectra of the PbSe polycrystalline films: (a) T_s = 250 °C and d_f varies as shown in the figure; (b) d_f = 3 μm and T_s varies as shown in the figure; the inset shows comparison between the experimental and theoretical substrate related interference fringes.

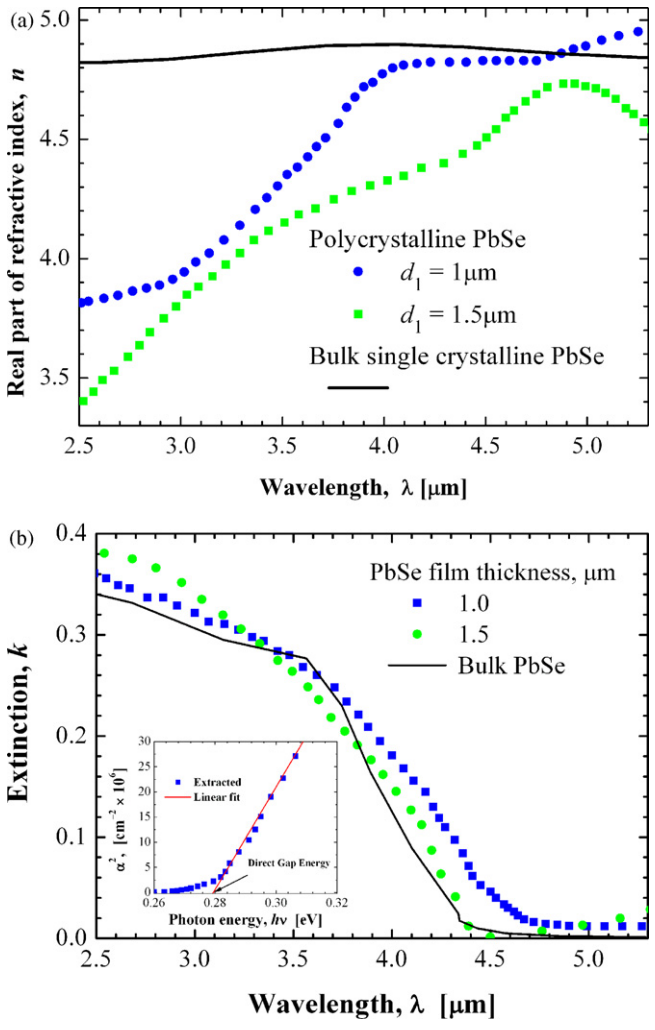

Fig. 7. The effective complex refractive index of the films with different d_f as shown in the figure, all grown at T_s = 250 °C; the full lines are the literature data for PbSe single crystal. The index extraction was performed as described in the text. (a) The real part n_1. (b) The imaginary part (extinction index) k_1; the inset displays the square of the absorption coefficient, thus obtained for the 1 μm thick film, versus photon energy.

tion in PbSe starts just below an edge of ~4.5 μm, it shows up in the transmittance spectra only for thick enough films as seen in Fig. 6(a). Two strong absorption bands at about 2.8 and 3.2 μm, clearly seen in Fig. 6(a), are wholly attributed to the polyimide.

Figs. 5(b) and 6(b) shows the evolution of the reflectivity and transmittance spectra, respectively, from 3 μm thick samples upon varying T_s. It is seen from Fig. 5(b) that the reflectance oscillations remain with the maxima and minima at about the same λ for all T_s, the reflectance level drastically decreases with decreasing T_s as it should occur due to the surface roughness enhancement trend discussed in Section 4.1. On the contrary, the normal transmittance is much less affected by the surface roughness as seen from Fig. 6(b). At the same time, lowering T_s leads to increasing the voids volume and hence the number of internal multiple scattering events, which changes the radiation transport from wave to diffusive like. As a result, the overall transmittance level notably lowers with the decrease of T_s, which is seen in Fig. 6(b).

The analysis based on Figs. 5 and 6 allows us to guess that in the light wave framework, the films grown at T_s = 250 °C are optically compatible to some homogeneous films. To support this idea we computed the $\mathcal{R}_a$ and $\mathcal{J}_a$ spectra using Eq. (6) and (7), respectively, for a homogeneous film with $d_1 = d_f = 1$ μm, and n_1 and k_1 equal those of crystalline PbSe [25]. The results are shown by the full lines in Figs. 5(a) and 6(a) in conjunction with the experimental data. Fair agreement between $\mathcal{R}_a$ and corresponding measured reflectance spectra as regards the oscillations maxima and minima positions is seen in Fig. 5(a). Moreover, the oscillation amplitudes are in a reasonable agreement at λ > 3.5 μm. As seen in Fig. 6(a), $\mathcal{J}_a$ and corresponding measured transmittance spectra are in overall fair agreement. This fact indicates a high precision in controlling the PbSe film thickness during growth.

Thus, we may assume that the noted films are well described by an effective complex homogeneous refractive index $n_1 + ik_1$ different from that of crystalline PbSe. To obtain the effective n_1 and k_1, we solved the inverse problem numerically using MATLAB. To this end Eqs. (6) and (7) were considered at each λ of interest as two equations for the two unknowns, in which $\mathcal{R}_a$ and $\mathcal{J}_a$ are substituted by the corresponding experimental data, and n_2, k_2 by the data obtained as described above. Since the effective complex refractive index of these films is not expected to diverge drastically from that of PbSe single crystal, we used the latter data as an initial guess. Fig. 7(a) and (b) shows the effective n_1 and k_1 spectra, respectively, thus extracted for two films with the thicknesses 1 and 1.5 μm together with the data for bulk [25]. It is seen in Fig. 7(a) that n_1 varies from film to film which is due to varying morphology. However, at 3.5 μm < λ ≤ 5.5 μm

the deviation from n_1 of PbSe bulk crystal is rather mild. As it appears from Fig. 7(a), at shorter wavelengths n_1 decreases much below the refractive index of bulk crystal, which is more pronounced for thicker films. This is likely due to contributions of light scattering inside the film, beyond a lowest-order effective medium theory (in which the optical permittivity is a mean of those over the grains and voids), which strongly enhances at λ/n_1, the wavelength inside the grains, approaching the grain size [18].

The extracted k_1 of the films proves very close to the extinction index of bulk PbSe crystal, as seen in Fig. 7(b), which may indicate that the voids' volume is relatively small. In addition, fitting the absorption coefficient, $\alpha_1 = 4\pi k_1/\lambda$, squared to a linear function of photon energy, shown in the inset to Fig. 7(b) yields for all the films grown at $T_s = 250\,^{\circ}\mathrm{C}$ about the same (effective) band gap energy ~0.28 eV which is pretty close to the value for PbSe single crystals [2]. This means that the grain size effects still do not influence much the inter-band optical transitions inside the grains. Below this edge, an additional absorption presents, for which the extracted k_1 increases with increasing λ. We explained this effect semi-quantitatively by free-carrier absorption via Eq. (2). For the films grown at other T_s, similar consistent description is not feasible due to large portion of the rough-surface scattering unaccounted by Eqs. (6) and (7).

5. Conclusions

Aiming at preparation of the polycrystalline PbSe films, in which strains are relaxed as much as possible, we proposed to use the polyimide substrate. Different PVD regimes, as regards the substrate temperature T_s and the film thickness d_f (i.e. the deposition time) in the range −50 to 350 °C, and 0.02–3 μm, respectively, were probed and the obtained films were characterized structurally, electrically and optically. As a whole, the growth of PbSe on the polyimide we carried out and the trends in the structural properties with the growth time and substrate temperature we observed, obey the regularities common for most polycrystalline films [21].

A series of the films deposited at $T_s = 250\,^{\circ}\mathrm{C}$ exhibited the best properties, including crystallinity of the grains, smallest surface roughness, and highest mobility in which temperature dependent part due to ingrain scattering of holes by phonons may be singled out. The IR optical properties of these films are plausibly described by effective-medium refractive index, while indicating the same band gap energy as in bulk single crystalline PbSe.

References

[1] R.G. Nimtz, B. Schlicht, Narrow-Gap Semiconductors, Springer Tracts in Modern Physics, vol. 98, Springer, Berlin, 1983, pp. 1–118.
[2] Yu.I. Ravich, in: D. Khokhlov (Vol. Ed.), M.O. Manasreh (Ser. Ed.), Lead Chalcogenides: Physics and Applications, Optoelectronic Properties of Semiconductors and Superlattices, Taylor & Francis, NY, 2002, vol. 18, pp. 3–30.
[3] A. Rogalski, Progr. Quant. Electron. 27 (2003) 59–210.
[4] D.L. Partin, IEEE J. Quant. Electron. 24 (1988) 1716–1726; H. Preier, Semicond. Sci. Technol. 5 (1990) S12–S20; H. Zogg, C. Maissen, J. Masek, T. Hoshino, S. Blunier, A.N. Tiwari, Semicond. Sci. Technol. 6 (1991) C36–C41.
[5] H. Zogg, in: D. Khokhlov (Vol. Ed.), M.O. Manasreh (Ser. Ed.), Lead Chalcogenides: Physics and Applications, Optoelectronic Properties of Semiconductors and Superlattices, Taylor & Francis, NY, 2002, vol. 18, pp. 587–615.
[6] P.R. Emtage, J. Appl. Phys. 47 (1976) 2565–2568; O. Ziep, M. Mocker, D. Genzow, K. H. Herrmann, Phys. Stat. Sol. (b) 90 (1978) 197–205; M. Mocker, O. Ziep, Phys. Stat. Sol. (b) 115 (1983) 415–425.
[7] R. Klann, T. Hofer, R. Buhleier, T. Elsaesser, J.W. Tomm, J. Appl. Phys. 77 (1995) 277–286; P.C. Findlay, C.R. Pidgeon, R. Kotitschke, A. Hollingworth, B.N. Murdin, C.J.G.M. Langerak, A.F.G. van der Meer, C.M. Ciesla, J. Oswald, A. Homer, G. Springholz, G. Bauer, Phys. Rev. 58 (1998) 12908–12915.
[8] Z. Dashevsky, in: A.A. Balandin, K.L. Wang (Eds.), Handbook of Semiconductor Nanostructures and Nanodevices, vol. 2, American Scientific Publishers, 2006, pp. 335–359.
[9] M.C. Torquemada, M.T. Rodrigo, G. Vergara, F.J. Sánchez, R. Almazan, M. Verdu, P. Rodríguez, V. Villamayor, L.J. Gomez, M.T. Montojo, J. Appl. Phys. 93 (2003) 1778–1784.
[10] Z.M. Dashevsky, M.P. Rulenko, Semiconductors 27 (1993) 366–368.
[11] S.V. Nepomnyashchii, A.V. Pashkevich, Yu.L. Shelekhin, L.K. Dilkov, Sov. Phys.-Semicond. 18 (1984) 1392–1393.
[12] A.E. Gamarts, V.A. Moshnikov, D.B. Chesnokova, Semiconductors 40 (2006) 662–664.
[13] M. Boberl, W. Heiss, T. Schwarzl, K. Wiesauer, G. Springholz, Appl. Phys. Lett. 82 (2003) 4065–4067; F. Zhao, S. Mukherjee, J. Ma, D. Li, S.L. Elizondo, Z. Shi, Appl. Phys. Lett. 92 (2008) 211110: 1–3.
[14] M. Rachim, A. Khiar, F. Felder, M. Fill, H. Zogg, Appl. Phys. Lett. 94 (2009), 201112: 1–4.
[15] A.M. Hermann, L. Fabick, J. Cryst. Growth 61 (1983) 658–664.
[16] http://www2.dupont.com/Kapton/en_US/assets/downloads/pdf/summaryofprop.pdf.
[17] M.S. Dresselhaus, Solid State Physics, American Scientific Publishers, 1980, Part 2. Optical Properties of Solids, pp. 110–130.
[18] D.J. Bergman, D. Stroud, in: H. Ehrenreich, D. Turnbull (Eds.), Solid State Physics, vol. 46, Academic, NY, 1992, p. 148.
[19] See e.g. M. Born, E. Wolf, Principles of Optics, Pergamon Press, Oxford, 1980; O.S. Heavens, Optical Properties of Thin Solid Films (reprint), Dover Publ., 1991.
[20] H.O. McMahon, J. Opt. Soc. Am. 40 (1950) 376–378.
[21] C.V. Thompson, Ann. Rev. Mater. Sci. 30 (2000) 59–190.
[22] J.N. Zemel, J.D. Jensen, R.B. Schoolar, Phys. Rev. 140 (1965) A330–A342.
[23] J. Wang, J. Hu, X. Sun, A.M. Agarwal, L.C. Kimerling, D.R. Lim, R.A. Synowicki, J. App. Phys. 104 (2008), 053707: 1–5.
[24] P. Sheng, B. Abeles, Y. Arie, Phys. Rev. Lett. 31 (1973) 44–46.
[25] N. Suzuki, K. Sawai, S. Adachi, J. Appl. Phys. 77 (1995) 1249–1255.